Geofísica Internacional (2005), Vol. 44, Num. 3, pp. 241-250

Multiphase flow reconstruction in oil pipelines by capacitance tomography using simulated annealing

R. Martin, C. Ortiz-Alemán and A. Rodríguez-Castellanos
Instituto Mexicano del Petróleo, México, D. F., México

Received: August 5, 2004; accepted: January 12, 2005

RESUMEN

En este trabajo un algoritmo de tipo recocido simulado (SA) altamente optimizado es aplicado a la reconstrucción de imágenes de permitividades a partir de datos de flujos difásicos reales cruzando una sección de un tubo cilíndrico usando tomografía de capacitancia eléctrica (ECT). La ECT proporciona imágenes de baja precisión comparando con otros procesos de tomografía, pero es robusta, barata y mucho más rápida. Este método no-intrusivo mide esencialmente distribuciones de permitividades en sistemas no-conductivos y se aplica en varios procesos de la industria petrolera como recipientes de mezclado, reactores de lechos fluidizados, tanques de separación o ductos transportando flujos multifásicos.

Para reconstruir las imágenes de flujos multifásicos a través de la sección de un contenedor cilíndrico, se determinaron las distribuciones de permitividad por medio de la tomografía de capacitancia eléctrica (ECT). Para este fin, un problema directo es resuelto en cada iteración de algoritmos de inversión de tipo recocido simulado "simulated annealing" (SA) y Landweber Proyectado. Pero se necesita todavía reducir el costo computacional de la resolución del problema directo a cada iteración de SA. Los métodos de Elementos Finitos o de Diferencias Finitas son generalmente escogidos para resolver el problema directo y los resolvedores de sistemas lineales introducen técnicas de diagonalización o de gradiante conjugado. En este artículo se introduce una discretización espacial por volúmenes finitos con refinamientos locales en una configuración cilíndrica con el fin de aumentar la resolución cerca de los electrodos, mejorar el cálculo de las capacitancias, y evitar problemas de resolución en el centro del sensor. Esta discretización tiene la ventaja de ofrecer una formulación conservativa usada en elemento finito y la flexibilidad para refinamiento de malla alrededor de los electrodos. De este modo se obtiene una mejor precisión local sin incrementar exageradamente el número de puntos de la malla. Los desempeños de la resolución del problema directo son analizados a la luz de los resultados obtenidos con métodos de elemento finito y datos experimentales. Se demuestra que la versión nonlineal de SA reconstruye mejor los flujos trifásicos que el método de Landweber.

PALABRAS CLAVE: Tomografía de capacitancia, recocido simulado, reconstrucción de imágenes, métodos de volúmenes finitos.

ABSTRACT

A highly optimized simulated annealing (SA) algorithm is applied to reconstruct permittivity images of real two-phase gas-oil flows through a cylindrical vessel using electrical capacitance tomography (ECT). ECT yields low-accuracy images but is robust, inexpensive and much faster than many other tomography processes. This non-intrusive method essentially measures non-conductive system distributions and is applied in oil industry processes such as mixing or stirring vessels, fluidized bed reactors, separator tanks and pipelines carrying multiphase flows.

A forward problem is solved at each step of an iterative algorithm to solve the inverse problem using simulated annealing (SA). Comparisons with linear methods like The Projected Landweber technique are discussed. In this paper we introduce a finite volume discretization with local mesh refinements in a cylindrical configuration close to the electrodes in order to improve resolution in the calculation of capacitances, and to avoid problems with resolution at the centre of cylindrical container when finite differences are used. This discretization has the advantage of a conservative formulation as used in finite element methods and features the flexibility of mesh refinement close to the electrodes. Thus, improvement of local accuracy is achieved without increasing prohibitively the number of mesh points. Performance of the forward problem resolution is compared with finite element based methods and experimental data. We show that the non linear version of SA provides better reconstructions of three-phase flows than the Landweber method.

KEY WORDS: Capacitance tomography, very fast simulated annealing, image reconstruction, finite volume method.

1. INTRODUCTION

Electrical Capacitance Tomography (ECT) is widely used in non intrusive tomography. ECT has been preferred over other tomography methods such as ultrasound, optical, X- and Gamma ray processes to obtain reconstructed images of multiphase flows in the inner core or region of a non conductive body. A review of the ECT systems was provided by Dickin *et al*. (1992). The first real-time ECT system was performed at the University of Manchester Institute of Science and Technology to visualize two-phase flow systems in pipelines (Huang *et al.,* 1992, Xie *et al*., 1992). Hardware

process systems based on similar concepts have since been developed using four to sixteen electrodes (Isaksen *et al*., 1993; Isaksen, 1996). Since 1995, process applications have increased and there has been significant improvement of design and operation of equipment (Beck *et al*., 1997). This non-intrusive technique is used to determine the permittivity distribution and composition of two-phase mixtures, like gas-solid or gas-oil systems. It has many useful applications in measurement of multiphase flows for the oil industry and more specifically in the study of oil-gas pipe flows, gas-solid distributions in pneumatic conveyors and fluidized beds, flame combustion processes, water oil-gas separators and trickle bed reactors for water content measurements (Yang, 1995a; Yang, 1995b; Yang, 2003).

As shown in Figure 1, an ECT multisensor is an insulating pipe surrounded by a circular array of electrodes in its outer boundary and by an external metallic screen which provides mechanical resistance to the whole sensor. By using cylindrical guards with a sufficient length, the sensor can model, by using a finite element method in the linearized forward problem solution, a two dimensional problem and visualize 2D averaged images (Xie *et al*., 1989). In this study n=12 fixed electrodes are considered around the sensor. Twelve successive excitations of the inner core of the sensor are performed with one (source) excited electrode and eleven non-excited (receiver) electrodes. The electrode 1 is excited and sends a positive potential field into the sensor and the induced capacitances received by the other eleven electrodes 2 to 12 are measured. Then the electrode 2 is excited and sends the electrical signal into the sensor while the other electrodes are not excited and are receivers, and the induced capacitances are measured at electrodes 1 and 3 to 12. This process is performed successively until the last electrode 12 sends the electrical signal and the induced capacitances are measured at the other non excited electrodes (receivers) 1 to 11. Thus, $m=n(n-1)/2=132$ capacitances have been measured. These mutual capacitances between every possible pair of electrodes, collected by the sensor, are measured by a connected electronic device. For n electrodes distributed around the cross-section to be studied, $m=n(n-1)/2$ electrode-electrode combinations are possible and m relevant mutual capacitance values are determined. These data are inverted by a suitable reconstruction algorithm which involves the resolution of a forward problem for each electrode problem. An image of the physical distribution of the different components of the mixture is provided into the sensor.

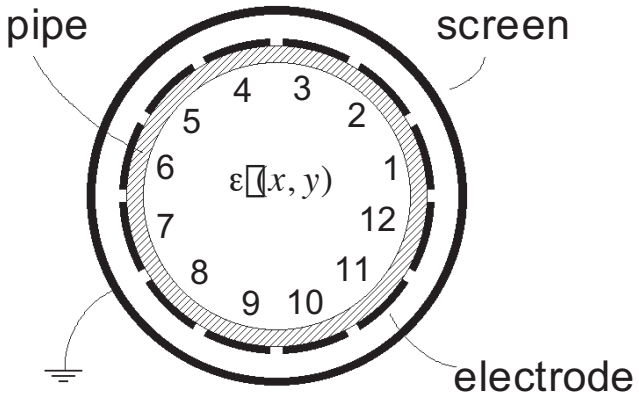

Fig. 1. Sensor cross section.

The main problem encountered by the commonly used image reconstruction algorithms has been their lack of reliability and accuracy. Simple direct methods like linear back-projection (LBP) only provide qualitative indications of the permittivity distribution inside the sensor. LBP is based on making a linear approximation to a problem that is essentially non-linear (Ortiz *et al*., 2003). Therefore, this image reconstruction method causes considerable errors, which are significant particularly if there are large permittivity differences in the image. A more accurate but much slower reconstruction technique is the use of iterative methods to minimize some objective function, employing local optimization techniques like the regularized Newton-Raphson method or other similar approaches (basically a Newton-type method with Tikhonov regularization) (Yang and Peng, 2003). These methods are based on minimizing, with respect to the permittivity distribution ε, a L^2 functional

$$\| C_{meas} - C_{calc} \|^2 + \alpha^2 \| \mathrm{M}\, \varepsilon \|^2 \qquad (1)$$

involving the misfit function between computed and measured mutual capacitances and a regularization matrix function M ε containing some type of *a priori* smoothness information about permittivities. $\mathbf{C}_{calc} = g(\varepsilon)$ is the vector of m computed mutual capacitances for a given vector ε.

Such iterative local optimization techniques generally require one or more regularization parameters whose optimal value depends precisely on the unknown image to be reconstructed. They smooth the whole image over some configurations where sharp permittivity contrasts are present, and sometimes they do not converge. This is mainly due to the fact that they perform local searches of the real solution around an initial guess which may be poor, particularly when flows moving with time are considered. Newton-Raphson methods (Hansen *et al*., 1998), Landweber techniques (Yang *et al*., 1999, Liu *et al*. 1999), steepest descent methods as well as the Algebraic Reconstruction Technique, the Simultaneous Iterative Reconstruction Technique (Reinecke and Mewes, 1996; Su *et al*., 2000), and iterative algorithms (Isaksen and Nordtvedt 1993) are often used. However, these methods may introduce undesired smoothing effects and instabilities in the reconstructed images. Regularization parameters depend on the image to be reconstructed. Thus the solution must be known beforehand. For a too strong regular-

ization smoothing effects will appear, and for a too slight one the technique becomes unstable and hardly converges. This is due to the fact that the reconstruction is non-linear and the linear algorithms previously mentioned are suitable tools for two phase flows but hardly apply for complex flows like bubbly or three phase flows (Peng and Yang, 2003). For more than two phases, the solutions converge towards the lowest and the highest boundary values allowable and then the other possible values are not well defined. This introduces bad contour definition and bad object dimensions because permittivities are adjusted to fit the objective function with only two possible values of the permittivities. These non-optimal solutions are computed because the global solution optima of the objective function are generally never reached.

According to Peng and Yang (2003), a compromise must be reached between fast algorithms and other algorithms much slower but more accurate, such as global non-linear methods. With local optimization, only a small set of solutions in the neighborhood of the initial solution is explored (Sambridge, 1992). A minimum of the objective function is searched during the iterative process and the lowest minimum is assumed to be the best model. But several local minima may be detected, and the optimal solution could be trapped and fail to converge. Least square linear methods are generally used and they introduce the objective function gradient in steepest descent or conjugate gradient algorithms.

On the other hand, a global optimization technique explores the full set of solutions during the iterative process. The objective function gradient is not needed because the problem does not need to be linearized. Stochastic criteria are introduced to explore simultaneously the space of solutions and find the optimal model. In particular, simulated annealing (SA) algorithms have proved to be efficient for many problems of interest in geophysics (exploration, magnetometry, gravimetry). These optimization systems take into account the previously evaluated models for each new model. They are based on Monte Carlo methods. Convergence of SA is achieved by means of a regularization procedure using cubic spline or median interpolations at each iteration of the inversion process. By this mean, the permittivity distribution is smoothed and numerical artifacts are avoided. Temperatures decrease also exponentially according to Very Fast Simulated Annealing versions proposed by M. Sen (Sen and Stoffa, 1995) instead of decreasing linearly. This acceleration allows a drastic decrease of the number of iterations of SA.

In this study we have chosen simulated annealing algorithm (SA) in order to obtain an accurate image of complex flows. The convergence of SA is highly dependent on the resolution technique employed in the forward (or direct) problem. SA can be identified as a non-linear multiparameter optimization method and a stochastic search technique which suites adequately to solve non linear problems like capacitance tomography. SA is also a generalization of Monte Carlo methods for examining the equations of state and frozen states of *n*-body systems (Metropolis 1953).

At each iteration of the SA algorithm, a forward problem is solved and fastened by using a finite volume method (FVM) and an Incomplete LU (ILU) preconditioned Bi-conjugate gradient (BiCG) solver. Here, different test cases showing representative permittivity patterns are presented. Here, the present study focuses essentially on the reconstruction of synthetic data. In the case of three different components (three different permittivities), we show that SA is able to reconstruct the three phases.

2. SIMULATED ANNEALING INVERSE METHOD

SA can be identified as a non-linear multiparameter optimization method. Such procedure is a stochastic search technique. SA is a powerful tool for locating an optimal model by rapidly exploring model space, it makes use of a stochastic search through model space employing a transition probability rule to improve the solution. The concept is based on the way liquids freeze or metals recrystalize in the process of annealing. In this process, an initially high temperature melt is slowly cooled down allowing the system to stay in thermodynamic equilibrium. As the process continues the molecules of the system tend to organize themselves towards a completely ordered arrangement which approaches to a frozen ground state.

The generalized extension of this approach to optimization problems can be easily formalized (Kirkpatrick 1983). To make use of the Metropolis algorithm, we followed the general procedure depicted in the layout of Figure 2. The atoms of each molecular configuration are equivalent to the model parameter in the inverse problem (i.e., the permittivity of the various image pixels). The energy of the system for such configuration is related to the cost function associated with the set of parameters involved in the model. In our case, the system energy is associated to the *L2* norm

$$E = \frac{\sum_{k=1}^{m}\left[C(k)_{meas} - C(k)_{calc}\right]^2}{\sum_{k=1}^{m}\left[C(k)_{meas}\right]^2} \quad (k=1,...,m), \qquad (2)$$

where $C(j)_{calc}$ are the m measured capacitances and $C(j)_{meas}$ are the ones calculated by solving the forward problem for a given permittivity distribution ε. From an initial permittivity distribution, the method generates a range of configurations or parameter combinations considering a certain temperature *T* for the process. For this purpose the Metropolis crite-

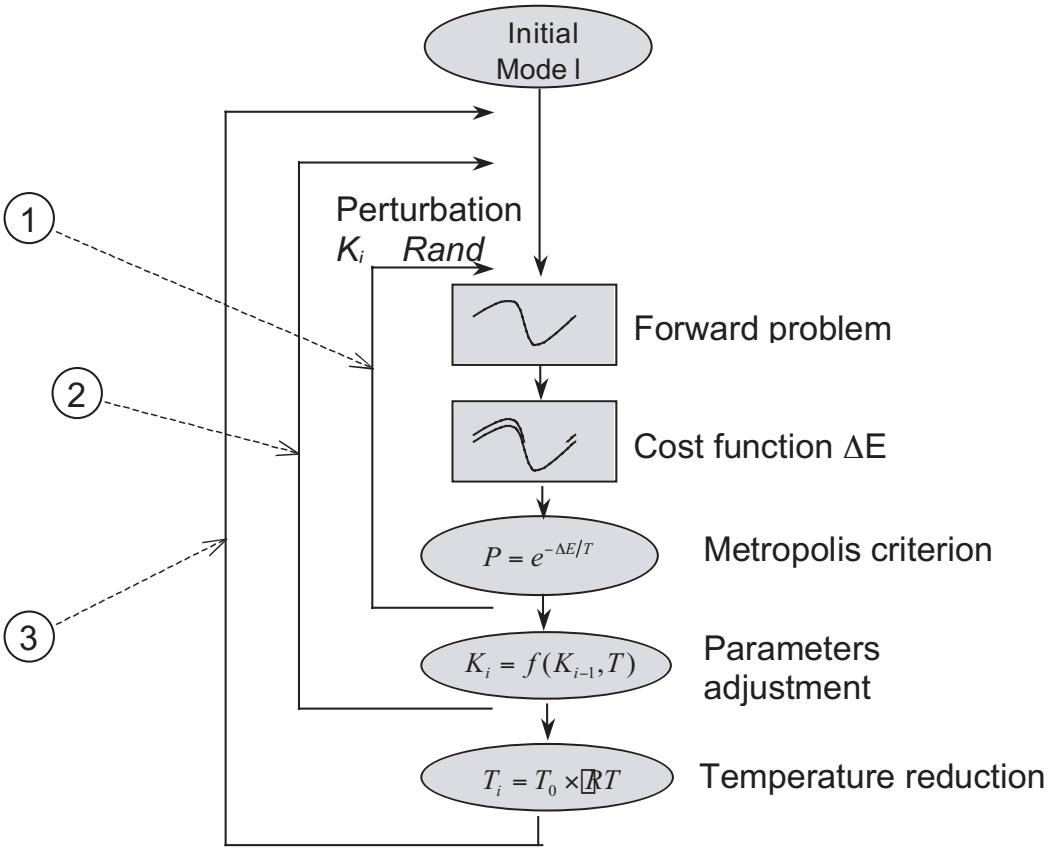

Fig. 2. Schematic diagram of the SA method.

rion is employed, which consists in changing a parameter, at each iteration, by a small random amount. This shift causes a change ΔE in the system's total energy. If ΔE is less than or equal to zero, the change in the parameter is accepted and the obtained configuration is considered as the new current configuration. When there is an increase in the system energy (ΔE is greater than zero), the probability of acceptance or rejection for the parameter change is determined as

$$P(\Delta E) = e^{-\Delta E/T}. \quad (3)$$

In order to decide whether or not a change that produces an increase in the system energy is accepted, a random number between zero and one is chosen such that it is compared with the value of the probability corresponding to ΔE. If the mentioned random number is smaller, the parameter shift is accepted and the new configuration is considered as an update. If the random number is greater, the parameter shift is not accepted and the configuration is unaltered. Repeating this procedure continuously, the thermal movement of the atoms of a system in thermal equilibrium (at a fixed temperature T) is simulated. In order to reach the system's base state, that is to say, the state of lowest energy and lowest disorder, the temperature must be reduced slowly, simulating a quasi-static process. This means that, along the cooling, the system must experience a series of states infinitesimally separated from the state of thermal equilibrium.

The process consists of three nested cycles. Figure 3 shows a diagram that illustrates how the method works. The external cycle regulates the system temperature. Every time a cycle is completed, the temperature decreases as it is multiplied by a factor RT that is normally very close to one ($0 < RT < 1$). In this way the desired slow and gradual cooling is carried out. The intermediate cycle updates the values, independent of each other, of a series of constants K_i associated with each parameter. Such constants determine the maximum change that each parameter may experience when it is perturbed in the innermost cycle. The value of the above mentioned constants depends on the number of times that the current model has been accepted (according to the Metropolis criterion) at the end of every sequence of internal cycles. In the internal cycle the parameter values are perturbed using the factors K_i, defined in the intermediate cycle. The perturbation is done multiplying each parameter by the product of its corresponding K_i times a randomly chosen number between minus one and one. After this, the synthetic response of the current model is calculated and the change in the system's energy associated with the new parameter configuration is evaluated. The energy change corresponds to the

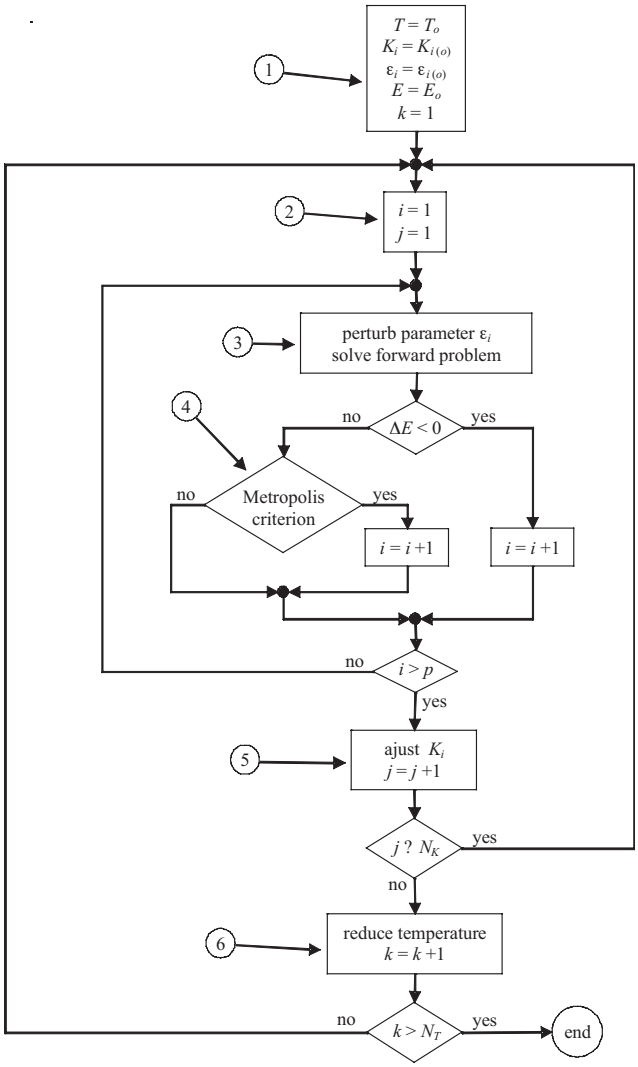

Fig. 3. A possible implementation of the SA method.

misfit between the synthetic data curve and the observed or measured one. If the misfit decreases, then the new configuration will be accepted as the current one and in turn perturbed in the same way. If, on the contrary, the random perturbation causes an increase in the misfit, associated with an increment in the energy E, then a slow probability of acceptance according to the Metropolis criterion is assigned to that configuration.

All three cycles are repeated, while the temperature of the process decreases progressively. As the temperature diminishes, the parameter variations are smaller. In this way, the search in the solutions domain tends to confine itself towards the models associated with the absolute minimum of the misfit function E. The final result is a set of values for the parameters (i.e., the permittivity in the various pixels that make an image) whose synthetic response reproduces the observed (capacitance) data, with a sufficiently small error.

The whole algorithm has been accelerated by using an exponentially decreasing temperature instead of a linear decrease in order to reach quickly an ideal temperature lying commonly between 10^{-8} and 10^{-9} for all the simulations. This version of SA is also called VFSA (very fast simulated annealing) and is inspired by the work of M. Sen and co-workers (Sen and Stoffa, 1995). Another optimization of the algorithm has been made by applying a smoothing of the parameters using bi-cubic spline or 6-point median interpolations every five external cycles of SA.

3. RESULTS

During the procedure for reconstructing a permittivity image using SA, it is necessary to solve the forward problem and find the electric potential repeatedly for relatively similar successive permittivity distributions, while the method converges towards the final solution. Since the potential corresponding to such successive distributions changes slightly, an iterative solver of the forward problem, like the bi-conjugate gradient linear solver, can be accelerated using the solution of the forward problem calculated at the previous iteration. The twelve potentials computed at the previous iteration of the inversion problem are set as first guess of the twelve new forward problems of the present new inverse problem iteration. The number of iterations per each forward problem is then quite random but always remains lower than the number of iterations at the first step of the whole inversion process.

Common finite element solvers like algorithm OPERA (Xie *et al.*, 1992) use matrix diagonalization and triangularization of the matrix system to be solved. The algorithm is not iterative and then three matrices are stored at each iteration of the inversion process. The algorithm is of order N^3 while the BiCG solver used here is of order N^2. The solutions obtained with the FE method are comparable to those of our FVM for a non-dimensional configuration. We have compared different profiles of the potentials using our FVM and the FEM along the radial direction for a given angle and two different grids (120 by 60 and 240 by 120 grid points). The finest grid gives us better results and the error between this grid and the FEM is relatively low and lies around 2%.

The errors between measured and calculated data can be really high with variations as important as 30% for the capacitances related to the receiver electrodes adjacent to the source electrode. This problem can be circumvented at the expense of a small loss of accuracy of the FVM and without increasing the number of mesh points. For this purpose, a multiplicative factor is applied to the calculated capacitances. This factor is directly related to an amount of error coming from well known measured and computed data in the case of an empty sensor (filled with air only). Without

changing the accuracy of the potential solutions in the sensor and without increasing the number of mesh points, the calculation of the capacitances is also improved by refining the mesh close to the electrodes and by increasing the radial spacing inside the sensor as shown in Figure 4. In order to show the accuracy of FVM, we plot in Figure 5, in a logarithmic scale, the errors between the FVM computed capacitances and the true data for an empty sensor configuration. Only one problem among twelve can be considered here because the other 11 problems are equivalent in this particular case. It is observed, as expected, that the worst errors between computed and measured capacitances are related to the electrodes (here electrodes 1 and 11) adjacent to the source electrode (here the electrode 12). The non-adjacent capacitances are really better computed.

In order to have a better resolution of the permittivity distribution, each parameter is chosen such that, in the inner core of the sensor, the patches related to each parameter have nearly the same size. Consequently, the impact of the different parameters is equivalent and the efficiency of the inversion process is improved because the intensity of changes in one parameter value is nearly the same for all the parameters during the iterative inversion process.

In order to test the feasibility of our SA inversion method, we computed sets of ECT synthetic data for four typical permittivity distributions by solving the forward problem. We simulated a twelve-electrode ECT sensor and computed the capacitance values for all single electrode combinations. For all the test cases, we considered two-component distributions with a lower permittivity material of 1.0 (air) and a higher permittivity material of 2.5 (oil). We restricted our numerical test to the reconstruction of noise free ECT data in the three first cases and we included random noise in the data for the fourth case. SA algorithm is implemented in Fortran 90 on a Pentium IV personal computer with a 1.7 MHz CPU and 512 Mbytes memory. We experimented with a 120 by 60 grid to reduce inversion times but results are valid for any larger dimensions.

After an adequate parameterization, SA produces satisfactory results for all four study cases. In Figure 6, we present image reconstructions for simple patterns as a stratified, an annular and a bubble flow 30 000 iterations of the SA process. The images are compared with those obtained with a Projected Landweber Method which gives us images after 500 iterations. We observe that SA gives better patterns, particularly in the stratified and the bubbly flow cases. The SA inversion of synthetic ECT data provides us very promising results but one of the drawbacks of the method is its relatively high computation time.

In the fourth case (three layer flow with permittivities of 1, 1.8 and 2.5), a model of our experimental sensor has been performed. The permittivities and the dimensions of each part of the sensor model as well as the electrode lengths (10 cm) are taken as realistic as possible. The insulated pipe of the sensor has a permittivity of 2.8 (acrylic). We compute the 132 synthetic capacitances C_{ij} for the 12 problems. By the theorem of reciprocity, half of the capacities are repeated twice so there are only 66 synthetic data to reproduce. These data are perturbed with a 10% random noise function in order to simulate a real case. The data with noise are inverted using the permittivity arrangement process described before with 240 patches. The images are very close to the image of

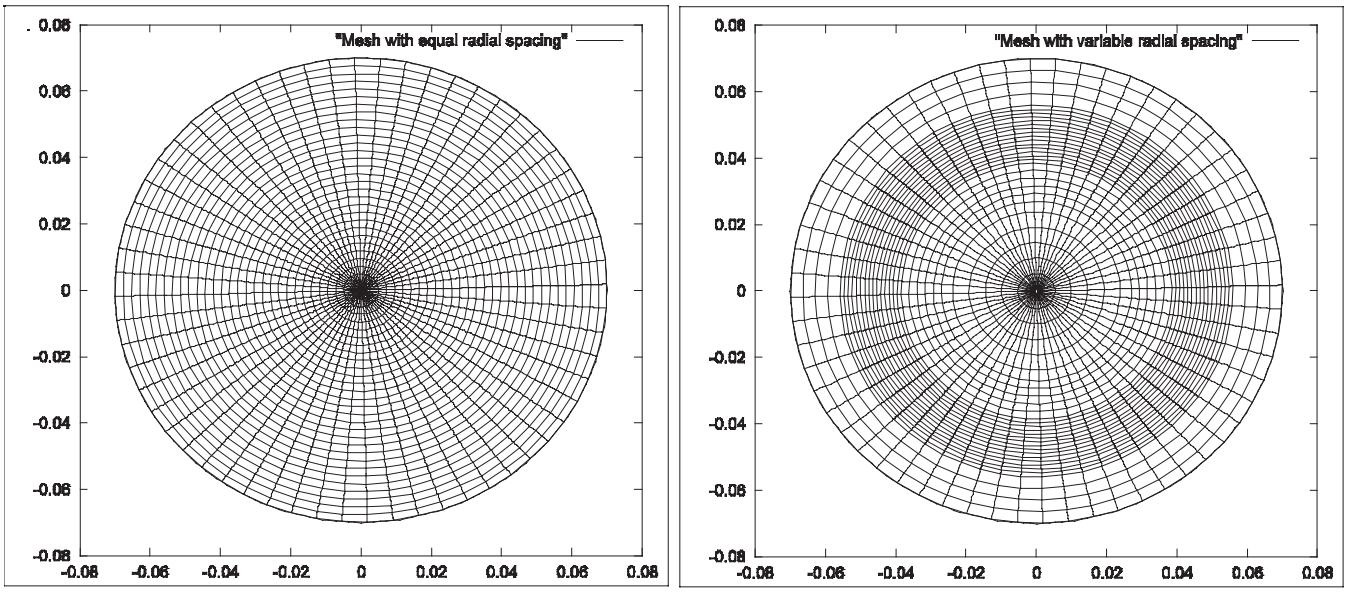

Fig. 4. Mesh with equal radial spacing (left) and mesh with different radial spacing used in this paper (right).

reference as can be seen in the snapshot of Figure 7. It is important to emphasize here that SA has been able to reproduce three different permittivities in the last case instead of two in the three previous cases. In Figure 7, the Landweber reconstruction gives a too much high permittivity in the top layer which is distorted. It is known that the linear local algorithms like LBP or Landweber do not give results with a good quality for three phases, as it is argued in the introduction of this paper. This is an advantage of SA upon Landweber. The SA algorithm converges towards an equivalent permittivity distribution and proves to be a good candidate for image reconstruction with random noise.

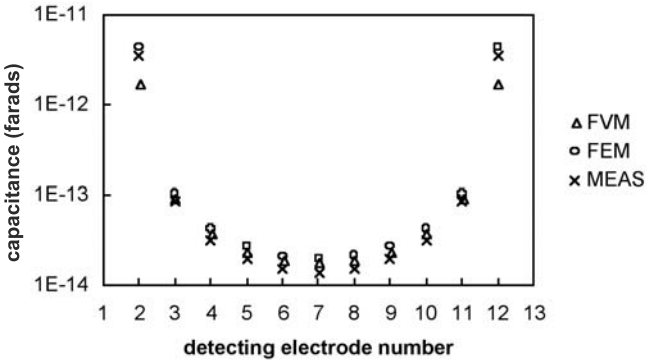

Fig. 5. Comparison between measured (MEAS) and calculated (using FEM and FVM) capacitance data between electrode 1 and each one of the eleven others for an empty 12 electrode realistic sensor.

For all cases, the imaging process using SA is stopped at 30 000 forward problem calculations. In a previous paper (Ortiz, 2003), we have shown that, during the 10 000 first iterations, the algorithm converges very fast then crosses a slow phase till 30 000 steps and accelerates until the process ends for a misfit function of approximately 10^{-6}. Here the Landweber's solution is combined with SA process so that the number of iterations of SA is drastically reduced to 30 000.

CONCLUSION

Applying SA to the inversion of synthetic data has given us promising results. The solutions are more accurate than those obtained with linear methods like LBP or Landweber. By introducing at each iteration of SA bi-cubic

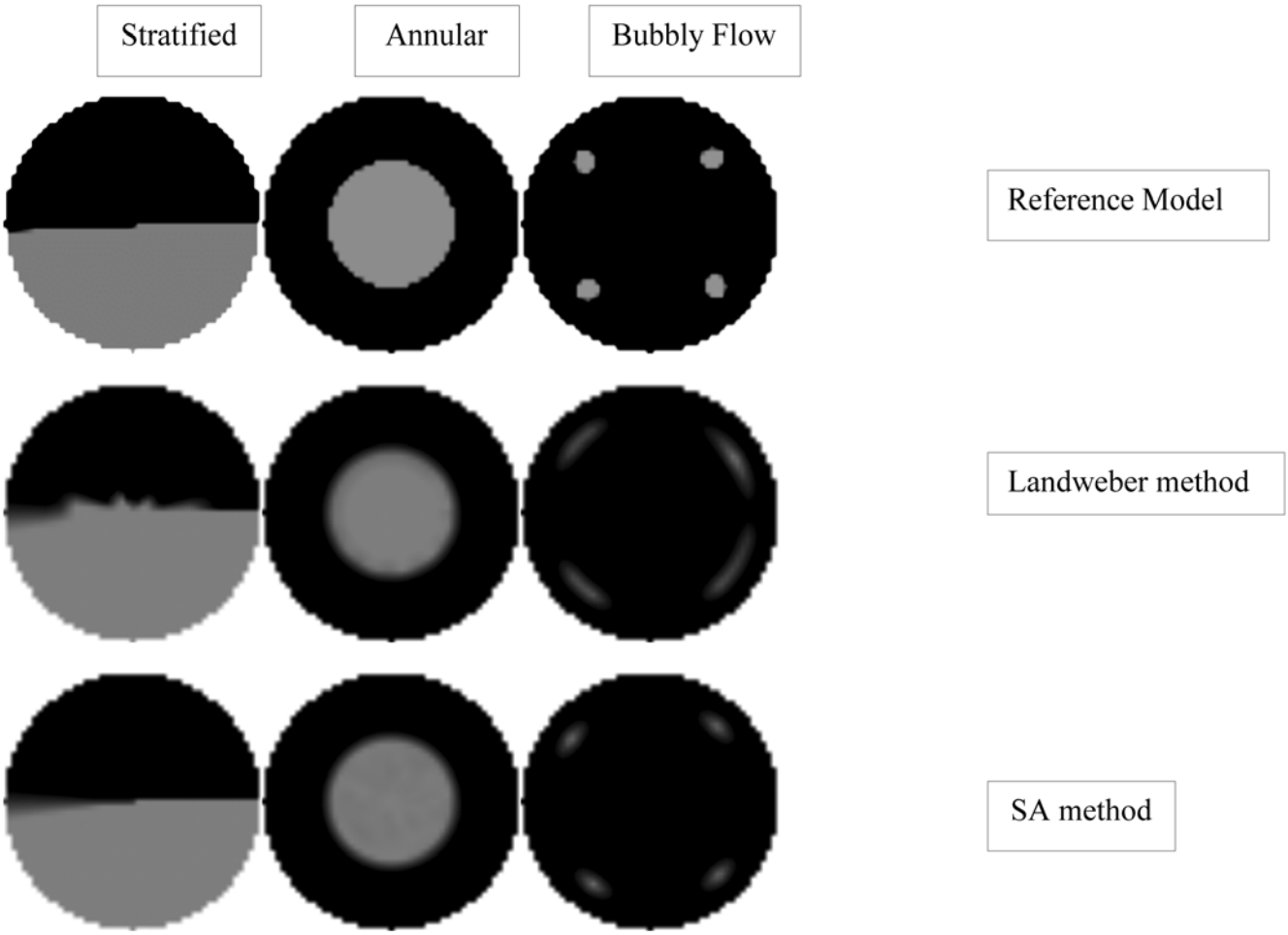

Fig. 6. Image reconstruction of synthetic ECT data for three typical test patterns assuming static fluids. Reconstructions after 1000 iterations of projected Landweber and 30 000 iterations of SA methods. White represents the permittivity of air and black the permittivity of oil.

spline or median interpolations of the parameters, the boundaries of the objects are better described by natural regularization. Of course SA using splines is a suitable alternative when better accuracy in image reconstruction is desired. However, the methods like SA are slower than less accurate methods like LBP. This iterative method does not need a good initial model to converge but it can be accelerated taking as a first guess the solution obtained by less accurate inversion methods. For instance, SA can be used as a post-processing procedure combined with LBP or different Landweber type algorithms.

Another way to accelerate the computational process, even in a high performance supercomputer, is to implement a linearized version of the forward problem. The capacitances at each iteration of SA could be calculated more easily by making the product of the new parameter change by the corresponding row of a sensivity matrix calculated at the beginning of the process. For real flows moving in time, the method can be fastened further by taking the previous solution as a first guess of the new solution to be calculated at a given instant. An exponential decrease of the temperature can be also introduced (Sen and Stoffa 1995) in order to reach rapidly ideal temperatures, allowing then quicker estimations of the solutions.

In order to compute real time flows, the linearized and non linear versions of the SA solver can be computed on a massively parallel computer like PC-cluster platform by solving in each processor one part of the sensor.

ACKNOWLEDGEMENTS

We thank W.Q. Yang for his fruitful discussions on linear inversion algorithms applied to capacitance tomography. The advice of M. Sen has also been very helpful for the implementation of the simulated annealing algorithm. This contribution was supported by projects IMP/D.00117 and IMP/D.00046.

APPENDIX

THE FORWARD PROBLEM SOLUTION

The forward problem consists in calculating the mutual capacitances C_{ij}, $i \neq j$, that result from the presence of a permittivity distribution e inside the sensor. The SA method requires the repeated solution of the forward problem. Because of that, it is important to have a suitable method to solve said problem, that achieves a reasonable balance between accuracy (or precision) and speed. In this paper, the forward problem was solved using an optimized routine based on the finite-volume method (FVM), which will be described briefly. This routine is very efficient and comparable in its precision with implementations based on the finite-element method (FEM) using meshes with 9000 triangular elements. The routine is written in Fortran 90 and is highly portable.

The use of the cylindrical axial end guards in the sensor, and the assumption that the phase (and thus the permittivity) distribution does not change too much in the axial direction, allow the sensor to be represented by a two-dimensional (2-D) model (Xie, 1989). The forward problem is solved using the finite-volume method in a cylindrical configuration. In this way, the undetermined solutions in the center of the disc (which are a problem in the finite difference method) are eliminated and the mesh refinement becomes more flexible as compared to finite-element methods. The following 12 2D-equations, describing the 12 different forward problems, are solved independently:

$$\nabla \cdot \varepsilon(x,y)\nabla\phi^{j} = 0 \qquad \text{j=1,…,12 ,} \qquad (5)$$

where ε is the permittivity and ϕ^{j} is the electrostatic potential distribution generated when electrode j is the source (or excitation) and the others are receivers (and not excited). Each equation j is subject to the boundary conditions $(a)\phi^{j} = V$ volts on the source electrode and (b)$\phi^{j} = 0$ on the detection electrodes and on the outer screen.

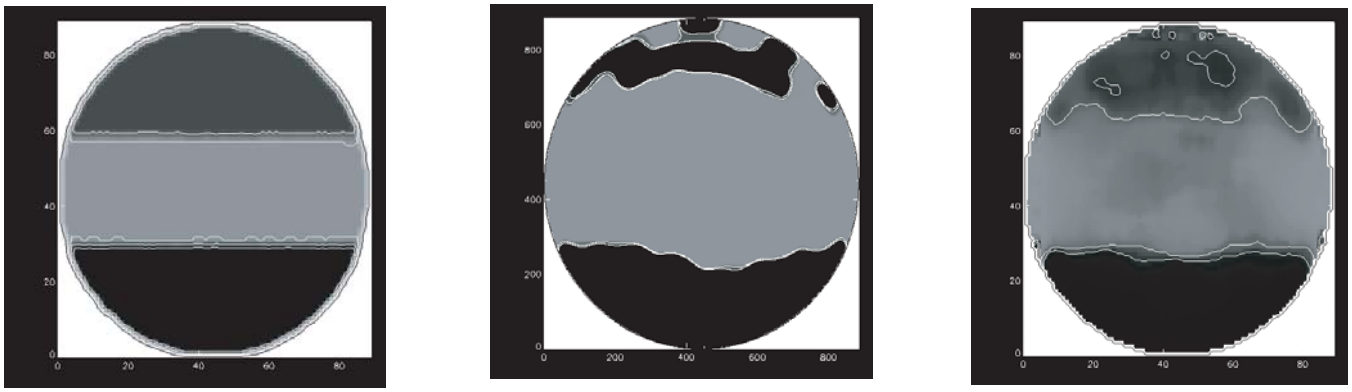

Fig. 7. Reconstruction of a three-layer flow with 10% noise in the data at 30 000 iterations. Reference model (left), linear Landweber reconstruction (middle), SA reconstructed image (right).

Defining the radial and angular coordinates as r and θ, and using the finite-volume method, the discrete equation is formulated in conservative form for each cell $\Omega_{\alpha\beta}$ as

$$\int_{\Omega_{\alpha\beta}} \nabla \cdot (\varepsilon \nabla \phi^j) d\Omega_{\alpha\beta} = 0 \text{ for } \alpha = 1,.., N_r \text{ and } \beta = 1,..,N_\theta \tag{6}$$

where the indexes α and β refer to the discretization in r and θ, respectively, and N_r and N_θ are the number of sections into which the radius and the circumference are divided, respectively.

Applying Gauss's theorem in polar coordinates, the discrete equations can be written as

$$\int_{\Gamma_{\alpha\beta}} \varepsilon \nabla \phi^j \cdot d\,\mathbf{\Gamma}_{\alpha\beta} = 0 \ , \tag{8}$$

where $\Gamma_{\alpha\beta}$ is the boundary of the finite volume cell $\Omega_{\alpha\beta}$. The boundary $\Gamma_{\alpha\beta}$ is defined by Γ_W and Γ_E along the radial coordinates, and by Γ_N and Γ_S along the angular coordinates. Equation (8) can be expressed as the sum of the fluxes through the faces Γ_N, Γ_S, Γ_E and Γ_W

$$\sum_l \left(\int_{\Gamma_l} \varepsilon \nabla \phi^j \cdot n_l d\,\Gamma_l \right) = \left(\frac{\varepsilon}{r} \frac{\partial \phi^j}{\partial \theta} \Delta r \right)\Bigg|_{\left(\alpha+\frac{1}{2}\right),\beta} - \left(\frac{\varepsilon}{r} \frac{\partial \phi^j}{\partial \theta} \Delta r \right)\Bigg|_{\left(\alpha-\frac{1}{2}\right),\beta} + \left(\varepsilon \frac{\partial \phi^j}{\partial \theta} r \Delta \theta \right)\Bigg|_{\alpha,\left(\beta+\frac{1}{2}\right)} - \left(\varepsilon \frac{\partial \phi^j}{\partial \theta} r \Delta \theta \right)\Bigg|_{\alpha,\left(\beta-\frac{1}{2}\right)}. \tag{9}$$

From equation (9), the term corresponding to the fluxes at zero radius vanishes and the problem is equivalent to solving the equations in the proximity of the center on triangles that have a vertex on the center. Then, the discrete system of equations for the forward problem is well posed. The complete system is similar to a Laplacian system of equations, and a diagonal banded system that includes the periodic boundary conditions imposed by the problem geometry must be solved. The corresponding matrix is positive definite and non-symmetric, characteristics that were exploited when selecting the biconjugate gradient method for its solution.

Finally, the mutual capacitances were calculated by integrating the potential gradients along a curve surrounding the electrodes, the following equation

$$\overline{C}_{ij} = \frac{Q_i}{V_j} = -\frac{\varepsilon_o}{V_o} \oint_{\Gamma_i} (\varepsilon \nabla \phi^j) \cdot d\mathbf{l} = -\frac{\varepsilon_o}{V_o} \oint_{\Gamma_i} \varepsilon \frac{\partial \phi^j}{\partial n} dl \ , \tag{10}$$

where n is the normal to the electrode contour, $\overline{C}_{ij}$ is the capacitance per unit length between electrodes i and j, Q_i is the electric charge per unit length induced on electrode j (the detection electrode), V_j is the voltage applied to electrode j (the source electrode), ε_o is the vacuum permittivity (8.854×10^{-12} farads per meter), Γ_i is a closed curve surrounding electrode i, $d\mathbf{l}$ is a normal vector representing an element of the curve Γ_i, dl is an elementary element of length of that curve and ϕ^j is the electrostatic potential distribution created in the sensor when applying a voltage V (volts) to electrode j (source) and 0 volts to all others (detection electrodes). The integration is performed using a trapezoidal rule and the potential gradients were calculated to the fourth order. The total capacitances C_{ij} are obtained multiplying $\overline{C}_{ij}$ by the electrode length, 0.1 meters in our case.

To accelerate the biconjugate gradient, we apply here an *ILU* precontionner to our non symmetric matrix solver. For this purpose, the matrix $\boldsymbol{A}^k$ describing each problem $\boldsymbol{A}^k\boldsymbol{\phi}^k=\boldsymbol{b}^k$ is split into $\boldsymbol{A}^k=\boldsymbol{M}-\boldsymbol{R}$ where the precontionner $\boldsymbol{M}$ is invertible and mimics the behavior of $\boldsymbol{A}^k$. The *ILU* factorization is as sparse as the lower triangular part of $\boldsymbol{A}$. It can be easily computed without much additional storage requirement because non-diagonal elements are the same as those of $\boldsymbol{A}$. Of course all the diagonal elements which intervene in the *ILU* factorization must be larger than zero, but in our finite volume approximation this is always verified, condition that is not verified for finite element methods (Wu, 2003). The number of iterations of the precontionned BICG code is less than the original and classical BICG version by a factor 3 (128 iterations instead of 450) for a solution error of 10^{-6} and the number of points chosen here.

BIBLIOGRAPHY

BECK, M. S., M. BYARS, T. DYAKOWSKI, R. WATERFALL., R. HE, S. M. WANG and W. Q. YANG, 1997. Principles and industrial applications of electrical capacitance tomography. *Meas. Control, 30,* 197-200.

DICKIN, F. J., B. S. HOYLE, A. HUNT, S. M. HUANG, O. ILYAS, C. LENN, R. C. WATERFALL, R. A. WILLIAMS, C. G. XIE and M. S. BECK, 1992. Tomographic imaging of industrial process equipment-techniques and applications". Proceedings IEE Part G, 139, 1, 72-82.

HANSEN, P.C., 1998. Rank-Deficient and Discrete Ill-Posed Problems. SIAM, Philadelphia.

HUANG, S. M., C. G. XIE, J. VASINA, C. LENN, B. F. ZHANG and M. S. BECK, 1992. Experimental evaluation of capacitance tomographic flow imaging system using physical models, Proc. 1st ECAPT Conf. (European Concerted Action on Process Tomography), Manchester, 26-29 March 1992, Ed. Beck M.S., Campogrande E., Morris M., Williams R.A. and Waterfall R.C. (Southampton: Computational Mechanics), 361-368.

ISAKSEN, O. and J. E. NORDTVEDT, 1993. A new reconstruction algorithm for process tomography. *Meas. Sci. Tech. 4,* 1464-1475.

ISAKSEN, O., A review of reconstruction techniques for capacitance tomography. *Meas. Sci. Tech., 7,* 325-37.

KIRKPATRICK, S., C. D. GELATT and M. P. VECCHI, 1983. Optimization by Simulated Annealing. *Science 220,* 671-680.

LIU, S., L. FU and W. Q. YANG, 1999. Optimization of an iterative image reconstruction algorithm for electrical capacitance tomography. *Meas. Sci. Tech. 10*, 37-39.

METROPOLIS, N., A. ROSENBLUETH, M. ROSENBLUETH, A. TELLER and E. TELLER, 1953. Equation of state calculations by fast computing machines. *J. Chem. Phys. 21,* 1087-1092.

ORTIZ-ALEMÁN, C., R. MARTIN and J. C. GAMIO, 2003. Application of simulated annealing and genetic algorithms to the reconstruction of electrical permittivity images in capacitance tomography. *In:* 3rd World Congress on Industrial Process Tomography, Banff, Canada, (CD Conference Proceedings).

REINECKE, N. and D. MEWES, 1996. Recent development and industrial/research applications of capacitance tomography. *Meas. Sci. Technol. 7,* 233-246.

SAMBRIDGE, M. and G. DRIJKONINGEN, 1992. Genetic algorithms in seismic waveform inversion. *Geophys J. Int. 109*, 323-342.

SEN, M. and P. L. STOFFA, 1995. Global Optimization Methods in Geophysical Inversion, Amsterdam, Elsevier.

SU, B., Y. ZHANG, L. PENG, D. YAO and B. ZHANG, 2000. The use of simultaneous iterative reconstruction technique for electrical capacitance tomography. *Chem. Eng. J. 77,* 37-41.

VASUDEVAN, K., W. G. WILSON and W. LADILAW, 1991. Simulated annealing static computation using an order-based energy function. *Geophysics 56,* 1831-1839.

WU X., 2003. A 3D finite element algorithm for DC resistivity modelling using the shifted incomplete Cholesky conjugate gradient method. *Geophys. J. Int 154,* 947-956.

XIE, C. G., A. PLASKOWSKI and M. S. BECK, 1989. 8-electrode capacitance system for two-component flow identification. Part 1: Tomographic flow imaging. IEE Proceedings A 136 (4), 173-183.

XIE, C. G., S. M. HUANG, B. S. HOYLE, R. THORN, C. LENN and M. S. BECK, 1992. Electrical capacitance tomography for flow imaging-system model for development of reconstruction algorithms and design of primary sensors. IEE Proc. G 139, 89-98.

YANG, W. Q., M. S. BECK and M. BYARS, 1995. Electrical capacitance tomography: from design to applications. Measurement and Control 28, 261.

YANG, W. Q., A. L. STOTT, M. S. BECK and C. G. XIE, 1995. Development of capacitance tomographic imaging systems for oil pipeline measurements. Review of Scientific Instruments 66, 4326.

YANG, W. Q., D. M. SPINK, T. A. YORK and H. MCCANN, 1999. An Image Reconstruction Algorithm based on Landweber's iteration method for electrical-capacitance tomography. *Meas. Sci. Tech. 10,* 1065-1069.

YANG, W. Q. and L. PENG, 2003. Image reconstruction algorithms for electrical capacitance tomography. *Meas. Sci. Tech. 14*, 1-13.

R. Martin, C. Ortiz-Alemán and A. Rodríguez Castellanos
Instituto Mexicano del Petróleo,
Eje Central Lázaro Cárdenas 152, 07730 México, D.F., México
Email: roland.martin@univ-pau.fr, jcortiz@imp.mx